

A Discrete Element study of the effect of particle shape on packing density of fine and cohesive powders

H.S. Elmsahli and I.C. Sinka*

University of Leicester, University Road, Leicester LE1 7RH

*corresponding author ics4@le.ac.uk

Manuscript submitted to Computational Particle Mechanics

21 February 2020

Abstract

Fine and cohesive powders typically exhibit low packing density, with solid volume fraction around 0.3. Discrete Element Modelling (DEM) of particulate materials and processes typically employ spherical particles which have much larger solid fractions (e.g. 0.64 for dense random packing of frictionless spheres). In this work a range of quasi-spherical particles are designed, represented by a number of small satellites connected rigidly to a larger centre sphere. Using DEM, packing density is found to be controlled by the interplay between particle shape, size and inter-particle cohesion and friction. Low packing density is obtained for an appropriate combination of 1) particle shape that allows the creation of geometrically loose structures via separation of the central particles by the satellites, 2) particle size that should be sufficiently small so that adhesive forces between particles become dominant over gravity, 3) adhesive forces, determined from surface energy should be sufficiently large, and 4) friction (static friction was found to have a dominant role compared to rolling friction, but negligible compared to adhesive forces for small particle size). By using the proposed quasi-spherical particle designs it becomes possible to calibrate more realistic DEM models for particulate processes that reproduces not only packing, but also other behaviours of bulk powders.

Keywords: Particle packing, shape, size, friction, adhesion, DEM

1.1 Introduction

The packing behaviour of particulate materials is of key importance in most manufacturing sectors for product and process design from bulk scale handling, transport and storage of particulate materials (energy, mineral processing, agriculture, construction) to the manufacturing of high value added complex formulated products and intermediaries (food, pharmaceuticals, detergents, speciality chemicals) and near net shape forming technologies (additive manufacturing, powder metallurgy, ceramics, hard materials) etc.

Unsurprisingly, particle packing has been studied extensively over many past decades and the first specialist reference book on particle packing was published by German in 1989 [1]. In the intervening period extensive studies have followed on the effect of particle physical characteristics (shape, size, and density), surface properties (affecting friction, adhesion) and contact interactions between particles on packing arrangement; the key findings are summarised below.

Particle arrangements can be categorised into two main types: ordered and random [1]. In theory, and according to [2, 3], the ordered packing of monosized spherical particles with an equal size can take several forms and the highest achievable solid volume fraction is 0.74 [4]. Random packing, on the other hand, presents a lower solid fraction which typically ranges between 0.60-0.64. The accepted solid fraction for dense packing is about 0.637 while 0.60 for loose random packing [1, 4].

Mixing two or more different sized particles leads to either increasing or decreasing packing density depending on the organisation of fine particles in the mixture. If the small particles occupy the interstitial voids between the large particles as shown conceptually in Figure 1a then the total space occupied by powder will decrease [5-8]. Alternatively, if the small particles are larger than the spaces between coarse particles or adhere to larger particles as illustrated in Figure 1b, then the packing density is reduced [1, 7].

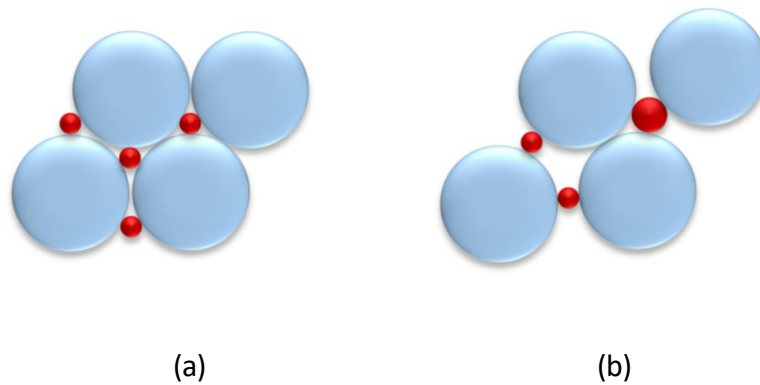


Figure 1 Conceptual illustration on possible packing arrangements of multi-sized particle assemblies, (a) increasing packing density, (b) reducing packing density

While particle size (or size distribution) is one of the key factors influencing packing density, it cannot fully explain the arrangements illustrated in Figure 1. By decreasing the particle size, below approximately 100 μm , packing density can be changed considerably [1, 9]. Due to the decrease of particle size, the specific surface area increases and the particle mass decreases. Consequently, the weak attractive forces such as electrostatic charges, capillary bridges, and van der Waals forces between particles become larger and more significant [1, 9-12] compared to gravitational and other inertial forces which are affected by density. With smaller particles, interparticle cohesion also increases and therefore agglomeration is likely to occur [9, 13].

Particle shape is also a key factor affecting packing. A number of studies conducted to establish relations between sphericity (particle roundness) and solid fraction [14]. Other authors [15-17] also highlighted the importance of sphericity and particle roundness for controlling the minimum and maximum solid volume fraction.

Irregularity of the particle shape influences interparticle friction and the more irregular the shape the lower the packing density [18-20]. In spite of spheres not being efficient geometries to fill a space (compared with e.g. cuboidal shapes), spherical particles facilitate rolling and rearrangement processes. The container wall used to hold the powder also influences the packing density by enabling unfilled low-density regions near to the wall. For binary mixtures with particle size ratios of less than 0.0035, however, the small particles form a monosized dense packing and wall effects become negligible [5].

1.1.1 Properties of fine and cohesive powders

Powders used in the manufacturing of pharmaceutical tablets, detergents, food products, fine chemicals, etc. are often composed of fine and cohesive particles. The packing of such powders is characterised by very low solid fractions. Handling and dosing operations takes place when the powders assume such loose packing arrangements. Taking some commonly used pharmaceutical excipients listed in Table 1 as example, their solid fraction in bulk state between 0.19 and 0.32, which is significantly lower than the loose random packing of spheres. The shape of the particles for the powders listed in Table 1 are illustrated in in Figure 2.

Table 1 Material properties for six pharmaceutical powders [21]

Material	Average particle size, μm	Bulk Density, kg/m^3	Bulk Solid Fraction
PH101	50	309	0.19
PH102	100	318	0.20
PH200	180	363	0.22
PH302	100	428	0.26
ATAB	180	725	0.25
Mannitol	180	498	0.32

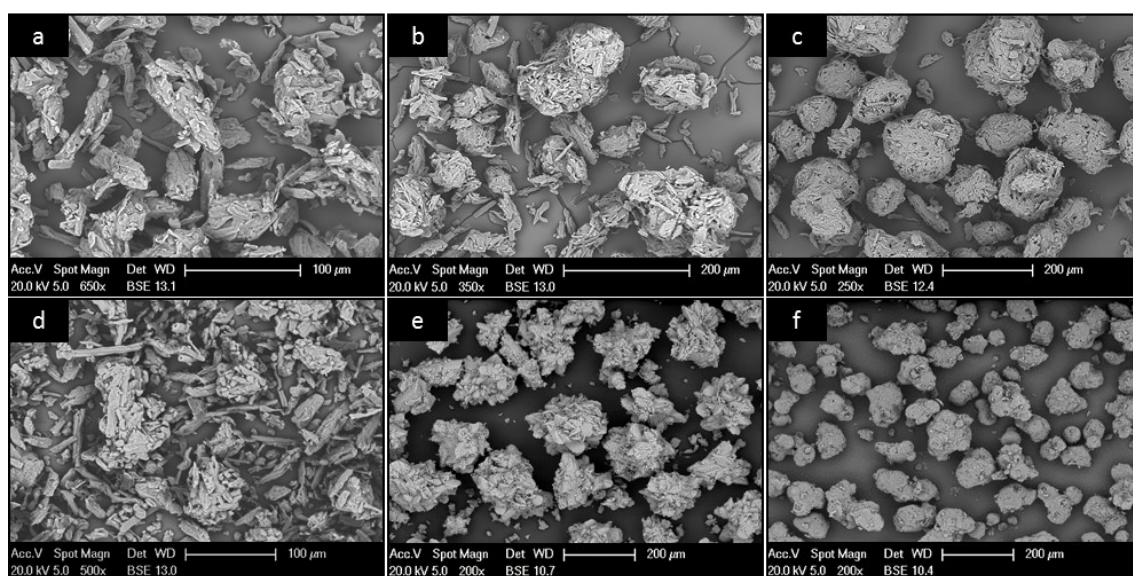


Figure 2 SEM images of pharmaceutical powders (a) PH101, (b) PH102, (c) PH200, (d) PH302, (e) ATAB and (f) Mannitol [21]

The discussion above shows that particle packing is determined by complex interactions between the physical characteristics of the particles and the details of particle interactions specific to different situations. Experimental observations using real particles led to detailed observations of the packing behaviour of different classes of materials. In recent years a complementary numerical technique, the Discrete Element Method (DEM), has been used to provide insight into the behaviour of particulate systems.

1.1.2 DEM analysis of particle packing

Discrete Element Modelling is becoming increasingly common due to steady advances in computational capabilities in terms of hardware and software. DEM opens virtual design possibilities for complex systems [22, 23] and is routinely applied across wide range of powder handling processes to simulate granulation [24, 25], die filling [26, 27], hopper discharge [28-30], segregation [31-33], in addition to particle packing [34, 35] and other applications.

DEM, also known as the distinct element method, was first introduced by Cundall and Strack [36] for simulation of jointed rocks. Since then, significant progress and development has been made in its methodologies and applications. In DEM every element represents one particle (grain). The movement of each particle is determined numerically through a series of calculations that trace each individual particle in a population of independent particles [37, 38]. When contacts occurs between particles, a local constitutive law (contact law) is employed to determine the contact forces which act on the particles and subsequently the motions of the particles involved in the contact [39].

The DEM algorithm includes an automated contact detection, which confirms formation or separation of the contact. The contact laws are the core ingredients of DEM and their validity determines the validity of the DEM simulation. Hertz-Mindlin contact model (non-linear elastic model) is one of the most commonly used contact force model in DEM to represent collision between non-cohesive spheres [40, 41]. In addition to contact forces, attractive particle interaction forces are usually taken into account in order to attain more realistic behaviour of cohesive systems. There are several options for handling cohesive particles in DEM simulations reported in the literature. The JKR model [42] is probably one of the most popular and widely accepted model used for modelling adhesive and fine particles [43-47] .

It follows that one of the critical aspect in powder simulations using DEM is the determination of the material properties and the contact interaction parameters [22, 48-50]. In order to produce accurate results that provide a realistic representation of the behaviour of the real material, the DEM requires that the input parameters are calibrated and validated [51, 52]. The calibration and validation strategies depend on physical nature of process being simulated which in turn corresponds to the behaviour of the actual bulk material [53, 54]. There are currently no universal or standardised calibration methods that can easily and effectively used to calibrate a bulk material for an arbitrary process [50, 54]. In general two approaches are followed for calibration of the DEM input parameters [22, 50, 55]. The first approach is typically achieved by experimentally characterising the behaviour of the bulk material. The experimental setup and procedures are then numerically replicated as closely as possible and the microscopic input parameters are adjusted iteratively until the DEM simulated results match the measured bulk behaviour using “trial and error” [50, 52, 55, 56] - this procedure can be effective for a given process, however, the parameters such determined cannot usually be used to model a different process involving different physics. In the second approach the input parameters are determined by directly measuring the values of material property (e.g. particle size, shape, friction, coefficient of restitution, and Young’s modulus) [22, 48, 50], then used to simulate bulk behaviour. The latter procedure is more suitable for spherical particles where it is possible to measure the particle properties.

In the current state of DEM modelling there are still some limitations and restrictions on the size, shape, and number of particles that can be simulated. Using the DEM approach for modelling a large number of irregular particles shape with small particle sizes makes computing time consuming [22, 57]. The majority of DEM simulations, therefore, consider using only a relatively small number of spherical particles in order to simplify the application and reduce the computation time [58, 59]. The representation of real particle shapes is still one of the key challenges that needs to be addressed during the simulation of granular material in order to obtain quantitative predictive accuracy for the modelled systems. Particle shape is an important factor which can be a dominant parameter in many cases. In dynamic systems, for instance (flow in hoppers or mixing applications), the particle shape controls the number of contacts and their trajectory which has a direct influence on the mechanisms of flow motion [28, 60]. Particle shape, in die fill and

compaction operations, as another example, affects the powder packing characteristics and therefore the volume and density of the bed occupied by the powder [61, 62].

Despite the fact that most real powders have large variations in particle size, shape and other characteristics the use of spherical particle shape is widespread in DEM because it requires only one size descriptor (particle radius) and it is convenient numerically for contact detection and calculation of contact forces. However, spherical shapes have inherent limitations for modelling the packing of real powder systems as exemplified below.

1.1.3 DEM analysis of particles with irregular shape

Inevitably, any DEM using spherical particles will suffer from the following limitation. The upper limit of dense random packing that can be obtained for frictionless spheres is of volume fractions with approximately 0.64 [63, 64]. The lower volume fraction for mechanically stable packings that can be attained for random loose packing in the presence of friction is around 0.55 [65-67]. This is notably different from the solid fractions of the typical powders used in the manufacturing of pharmaceutical tablets, detergents, food products, fine chemicals, etc.

There are several methods that have been proposed in literature to represent complex and non-spherical shapes. One of the simplest and most commonly used is the multi-sphere method which treats one or more sets of particles as independent bodies formed by multiple spheres joined rigidly together [68]. By increasing the number of spheres more complicated shape envelopes can be created with increasing refinement. The properties of individual multi-sphere bodies (often referred to as “clumps”) are calculated and updated at each time-step. The kinetic and rotational energy of each rigid body is updated based on its centre of mass so that the whole body moves and rotates as a single entity. The total force and torque acting on each multi-sphere body is calculated as the sum of the forces and torques on its forming particles and the coordinates [68-70]. However, a significant drawback related to this method, is the increase of computational memory requirements with the increase of precision requirements for the represented complex shape. In addition it is difficult to approximate shapes having sharp edges and large aspect ratios [22].

Nevertheless, recent improvement in computational power and increasing of memory capacity enabled numerous studies of packing of complex shaped particles using multi-sphere methods targeting different industrial applications. Deng and Davé [47], for instance, used the multi-sphere

method with the JKR model to investigate the effect of the particle size, aspect ratios (0.0, 1.0, and 3.0), and cohesiveness on the packing structure. They demonstrated that the porosity decreases with increasing particle size for the case of non-zero surface energy; whereas the porosity becomes significantly higher (as high as 0.83) for finer particles in the presence of cohesive force with the increase of aspect ratios. Other authors used the same method to study the packing density of ellipsoid particles. You and Zhao [71] used DEM to investigate the packing and flow behaviour of ellipsoidal particles and they documented solid fraction in the range of 0.542 - 0.587. He et al. [72] examined the effect of the initial packing on the compactions of spheroidal particles of different aspect ratios. They highlighted that the solid fraction increases with the aspect ratio and reaches a maximum of 0.685 at a ratio of 0.75. It then decreases with increasing aspect ratio and has a minimum of 0.63 when the ratio is 1 (spheres). There are several other methods and techniques that can be found in the literature which used to model and study packing of non-spherical particles [73-77].

Clearly, particle shape has a key influence on packing. However, packing is also controlled by the effect of friction, surface energy, etc. DEM results can also be manipulated by changing the initial conditions of the particles (the so-called particle "insertion"). For packing of spherical particles, for instance, even though the random close packing is around 0.64, some studies [78-80] demonstrated that the solid fraction of spherical particles can be reduced to be as low as 0.22-0.154 by increasing the work of adhesion. Liu, Li [79], for instance, showed that increasing the size of spherical particle from 1 μm to 10 μm of the same surface energy and under the same insertion conditions increase the solid fraction almost two folds. However, these systems are unstable: during the DEM initialisation procedure, by increasing the insertion velocity from 0.5 m/s to 6 m/s the solid fraction almost trebled. This type of structure is unstable for many applications especially that involve particle movement (e.g. powder flow). Therefore, obtaining packing densities as low as in Table 1 for a stabilized loose particle packing with spherical-like particle shape remains a challenge.

Spherical shapes offer advantages in terms of modelling processing, transport and handling (e.g. high packing density, good flow properties etc.). Practical particles, are, however, mostly irregular and usually the greater the shape irregularity the lower bulk density that can be obtained [14, 16, 17]. Ceramic particles (e.g. Figure 2e) or particles obtained through crystallisation (e.g. Figure 2f) are inherently faceted. Metal or polymeric particles made through atomisation processes are also

mostly irregular although spherical shapes can be also engineered at a cost. In most practical processing situations the reduction of fines is desired and round particle shapes are preferred, for this reason many practical powders are agglomerated into larger, quasi-spherical granules as shown in Figure 2.

1.1.4 Purpose of the paper

The majority of DEM work reviewed above uses a calibration procedure to derive effective properties for the particles which are then used as DEM inputs to reproduce a given process. The problem with this approach is that effective properties calibrated for one process may not describe the behaviour of the same powder under a different process. The solid volume fractions of a loose random packing of spheres is above 60%. As described above, by manipulating the friction and adhesion behaviour it is possible to obtain looser packing, but these would collapse into much denser packing if subject to handling conditions. Also, as seen above, it is possible to scan real particles using X-ray CT and digitise for DEM use. Commercial software exists for faceted particles, etc. The practical problems associated with modelling realistic particle size distributions (fines in particular) still remain even when 100million particles are perfectly possible.

The purpose of the paper is to design an effective particle shape that is equivalent to the real powders in Figure 2 that can be used to describe multiple different processes involving fine and cohesive powders. In this paper we focus on packing. Forthcoming work [Elmsahli and Sinka, IJSS, under review] describes the use of these shapes to capture other behaviours, including permeability, angle of repose and flow under differential air pressure.

The principle behind the design of the equivalent particle shapes is presented in Figure 1. Essentially, the complex shapes are created using the clumped sphere method, with a large central particle surrounded by satellites. The principal role of the satellites is not to mimic the shape of real particles, but to keep the large central cores apart thus achieving low packing density. A series of quasi-spherical particles composed of a central sphere surrounded by satellite particles arranged in a dodecahedron pattern are designed. Diameters of the order of hundreds of micrometres are considered. The role played by particle shape, size, adhesion and friction is demonstrated. It is shown that using appropriate quasi-spherical particle shapes together with adhesion and friction interactions DEM can reproduce the low packing density of fine and cohesive powder systems.

1.2 DEM model implementation

The DEM studies are carried out using the open source DEM code LIGGGHTS running on the University of Leicester HPC cluster. A typical study involved 20,000 multi-sphere particles (140,000 -300,000 single particles) and was run on 16 processors requiring 3-14 hours depending on the particle size. Therefore for practical considerations the number of studies were limited to a few hundred of simulations and the parametric studies were designed accordingly.

The packing behaviour is affected by adhesive forces between particles which depend on particle size. When reducing particle size, the size of the domain was reduced accordingly to keep the number of particles the same.

The non-linear Hertzian elastic contact model for frictional force between particle-particle and particle wall was used as implemented in the code (LIGGGHTS).

$$F = (k_n \delta n_{ij} - d_n V n_{ij}) + (k_t \delta t_{ij} - d_t V t_{ij}) \quad (1)$$

The first and the second term in the above-equation represent the normal (F_n) and tangential force (F_t) respectively.

The normal (k_n) and tangential stiffness (k_t) are calculated from the material properties as follows according to the contact model presented by Thornton et al [81] for the non-linear spring-dashpot model presented in Figure 3 :

$$k_n = \frac{4}{3} E^* \sqrt{R^* \delta_n} \quad (2)$$

$$k_t = 8 G^* \sqrt{R^* \delta_n} \quad (3)$$

where E^* and G^* are the effective Young's and shear modulus respectively, and R^* is effective radius. These terms are given by:

$$\frac{1}{E^*} = \frac{(1 - \nu_i^2)}{E_i} + \frac{(1 - \nu_j^2)}{E_j} \quad (4)$$

$$\frac{1}{G^*} = \frac{2(2 - \nu_i)(1 + \nu_i)}{E_i} + \frac{2(2 - \nu_j)(1 + \nu_j)}{E_j} \quad (5)$$

$$\frac{1}{R^*} = \frac{1}{R_i} + \frac{1}{R_j} \quad (6)$$

where the indices correspond to the properties of particles labelled P_i and P_j in Figure 3.

The normal (d_n) and tangential viscoelastic damping coefficients (d_t) are calculated using:

$$d_n = -2 \sqrt{\frac{5}{6}} \beta \sqrt{S_n m^*} \geq 0 \quad (7)$$

$$d_t = -2 \sqrt{\frac{5}{6}} \beta \sqrt{S_t m^*} \geq 0 \quad (8)$$

where β is the dimensionless damping coefficient governed by coefficient of restitution (e) and m^* is the effective mass. These parameters including S_n and S_t are defined as follows:

$$\beta = \frac{\ln(e)}{\sqrt{\ln^2(e) + \pi^2}} \quad (9)$$

$$\frac{1}{m^*} = \frac{1}{m_i} + \frac{1}{m_j} \quad (10)$$

$$S_n = 2E^* \sqrt{R^* \delta_n} \quad (11)$$

$$S_t = 8G^* \sqrt{R^* \delta_n} \quad (12)$$

275

276 In this model the tangential force is limited by Coulomb friction ($F_t = \mu F_n$). Thus the tangential
277 force between two particles grow according to a tangential spring and dashpot model
278 until $F_t/F_n = \mu$ (*Static friction* coefficient) and is then held at $F_t = \mu F_n$ until the particles
279 lose contact.

280 As a part of Hertz model there are also other models that can be used to add additional forces or
281 torques on the particles, such as cohesive or rolling friction forces. These models can be activated
282 or deactivated depending on the user's needs. For example, there are four different
283 implementation models for rolling friction that can be used as a part of Hertz model to add an
284 additional torque contribution. These models referred to as the constant directional torque (CDT)
285 model, the elastic-plastic spring-dashpot (EPSD) model, the alternative elastic-plastic spring-
286 dashpot (EPSD2) model, and the elastic-plastic spring-dashpot (EPSD3) model. The first model
287 (CDT) was used in this study and it is defined as:

$$\text{Torque rolling friction} = \mu_r * k_n * \delta_n * (\omega_{rt} / |\omega_{rt}|) R^* \quad (13)$$

288

289 Where μ_r = coefficient of rolling friction and ω_{rt} = shear relative rotational velocity between
290 two particles.

291 LIGGGHTS also has various cohesive models that can be used to add additional forces to Hertzian
292 model. Such cohesion models may impose a force also when the particle surfaces do not touch.
293 These models include sjkr model, sjkr2 model, easo/capillary/viscous model, and cohesion
294 washino/capillary/viscous model. The latter two models are used as part of Hertz model to add a
295 liquid bridge force between a pair of particles caused by a surface liquid film on these particles.
296 The former two models, which are referred to as the simplified JKR - Johnson-Kendall-Roberts
297 (SJKR and SJKR2), on the other hand are used to add an additional normal force contribution and
298 written as:

$$F = kA \quad (14)$$

299

300 where A is the particle contact area and k is the cohesion energy density in J/m³. The sphere-
301 sphere contact area "A" is defined differently on those two models depending on the selected

cohesion model. Both these models were using the concept of cohesion energy density (CED) instead of surface energy to determine the cohesive force. The values that used with CED are different form the common surface energy values which are usually used with granular materials. Therefore to conduct this study using surface energy definition a JKR model was implemented into the code which takes the following format:

$$F_{JKR} = -4\sqrt{\pi\gamma E^*} a^{3/2} + \frac{4E^*}{3R^*} a^3 \quad (15)$$

$$\delta = \frac{a^2}{R^*} - \sqrt{4\pi\gamma a/E^*} \quad (16)$$

where a is the contact radius and γ is the surface energy. For $\gamma = 0$ force turns into Hertz normal force. Equation (15) was implemented in LIGGGHTS and the implementation was validated as presented elsewhere [82].

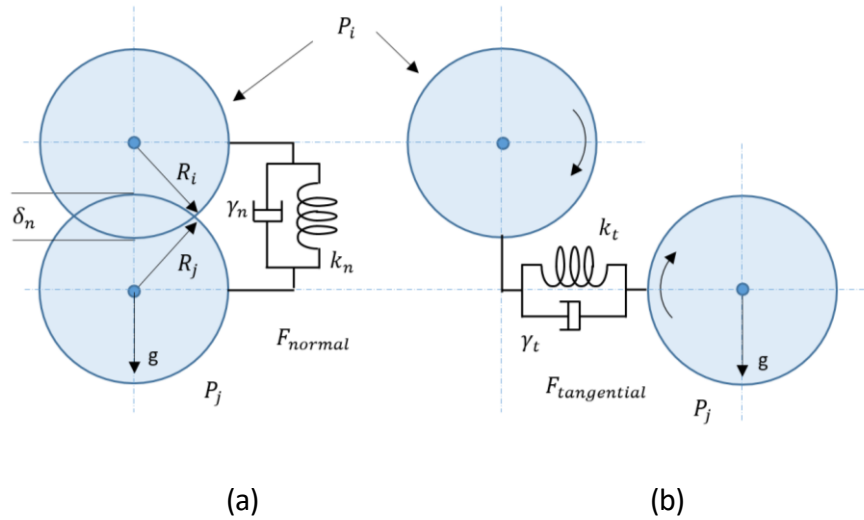


Figure 3 Linear spring contact model in (a) normal and (b) tangential direction of contact of two particles.

DEM analysis of particle packing involves the following steps: 1) creating a domain (for the current study a square cross-section of 5x5 mm and height of 50 mm is considered); 2) defining the size and shape characteristics of the particles; 3) initialising a cloud of a given number of

particles and 4); allowing the particles to fall under gravity and settle in an equilibrium configuration. The solid volume fraction of the final assembly is then determined.

In order to reduce wall effects arising from friction and adhesion between the particles and the walls periodic boundary conditions are specified along the two horizontal directions of the domain.

The particle packing was characterised by determining the solid volume fraction (SF) of the domain using one of the following two methods: 1) measuring the height of an assembly consisting of a given number of particles and 2) counting the particles occupying a volume of a given height. In both cases the volume occupied by the solid is calculated by multiplying the volume of one particle by the number of particles in the system as illustrated in Figure 4.

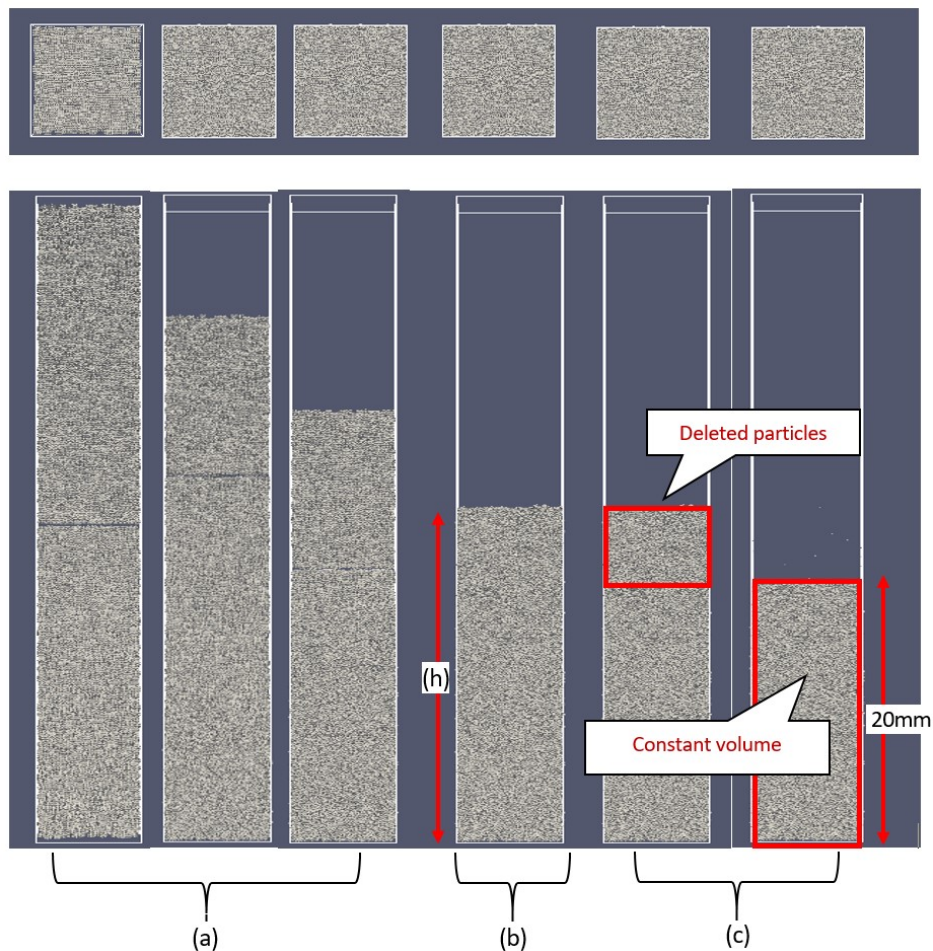


Figure 4 Particle insertion and solid fraction determination. a) initial particles insertion, b) determination of SF based on the settled powder height, and c) determination of the SF based on a constant volume. The squares at the top illustrate the cross-section of the domain.

1.3 Model input parameters

1.3.1 Particle shape design

In the following we construct particle shapes using the multi-sphere method by considering a central sphere surrounded by smaller overlapping particles arranged in regular dodecahedron pattern. In the arrangements in Figure 7 satellite spheres are placed such that their centres are on the surface of the central sphere.

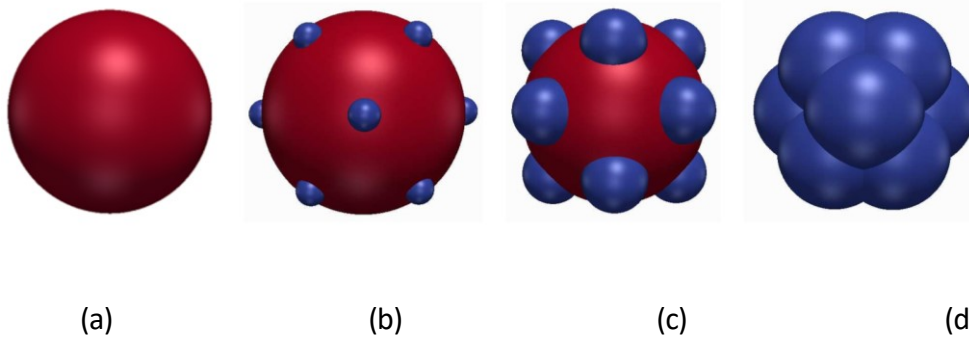
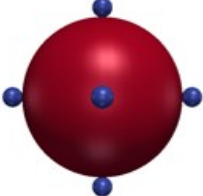
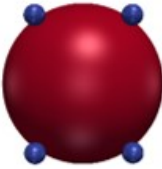
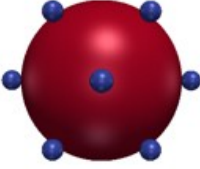
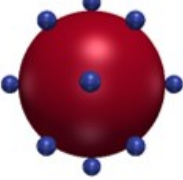
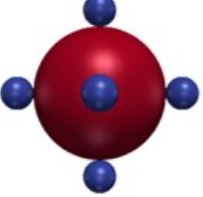
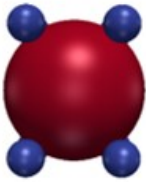
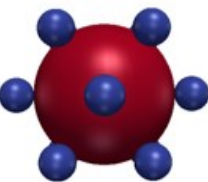
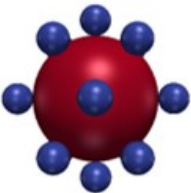
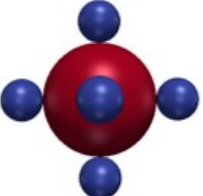
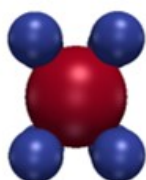
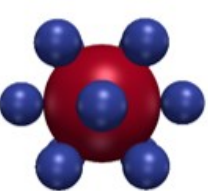
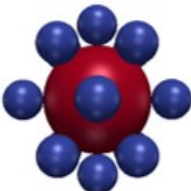
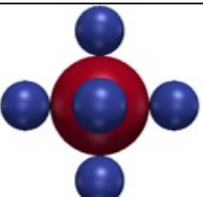
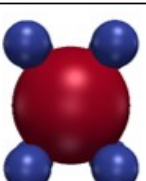
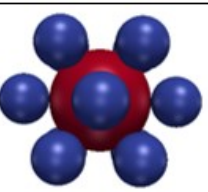
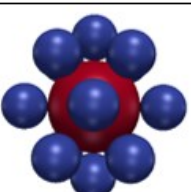
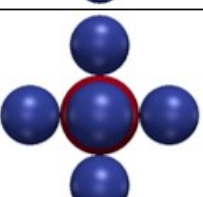
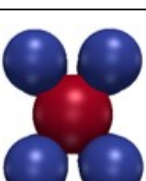
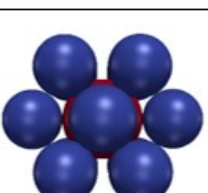
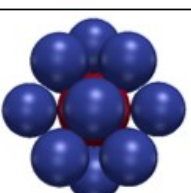
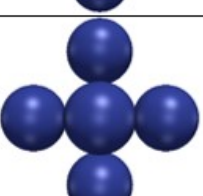

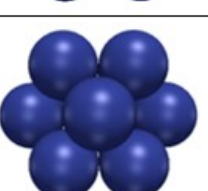
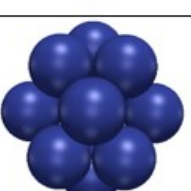


Figure 5 Multi-sphere particle based on small overlapped particles (External diameter 400 μm). a) 400 μm , b) 350 and 50 μm , c) 300 and 100 μm and d) 200 and 200 μm for the central sphere and the satellite particles, respectively.

It will be shown later (Section 1.3.1) that particle designs such as in Figure 5 produce assemblies where the packing density is reduced from 0.52 to about 0.455; however, packing assemblies of the order 0.2-0.3 cannot be achieved with such designs.

In order to obtain lower particle packing, in the following particle designs the satellite particles are translated outwards until the overlap with the central sphere is reduced to the point of contact. It will be shown later that this results in lower packing density values, in the practical range presented in Table 1. Table 2 presents the particle designs used for detailed studies in this work.

Table 2 Particle shape design

Particle diameter (Scale)	Shape 1	Shape 2	Shape 3	Shape 4
	1 Large particle + 6 Small	1 Large particle + 8 Small	1 Large particle + 12 Small	1 Large particle + 14 Small
Size 1 4 & 0.5				
Size 2 4 & 1				
Size 3 4 & 1.5				
Size 4 4 & 2				
Size 5 4 & 3				
Size 6 4 & 4				

353

354 1.3.2 Particle size description

355 Particle size is one of the key descriptors of powders and has a key influence on bulk properties.
356 Describing the size of irregularly shaped particles is a branch of science in itself. Although the quasi
357 - spherical shapes of the particles used in this study are based on a regular arrangements, detailed
358 considerations are needed to define particle size.

In practice, there are several different methods used to derive an equivalent size for an irregular particle. These methods include (1) using a sieve to measure the equivalent spherical particle that passes through a given sieve aperture; (2) using the sedimentation technique to find the equivalent diameter of spherical particle that give the same sedimentation velocity under the same conditions; (3) measuring the projected area or distance between two tangents on opposite sides of the particle (microscope analysis); and (4) finding the equivalent sphere that gives the same particle volume [83], which is in fact one of the most commonly used method.

Consider a multi-sphere particle consisting of one central sphere of 100 μm diameter surrounded by 12 small particles with 50 μm diameter. Figure 6a illustrates the envelope external diameter, Figure 6b shows the diameter to the centre of the satellite particles.

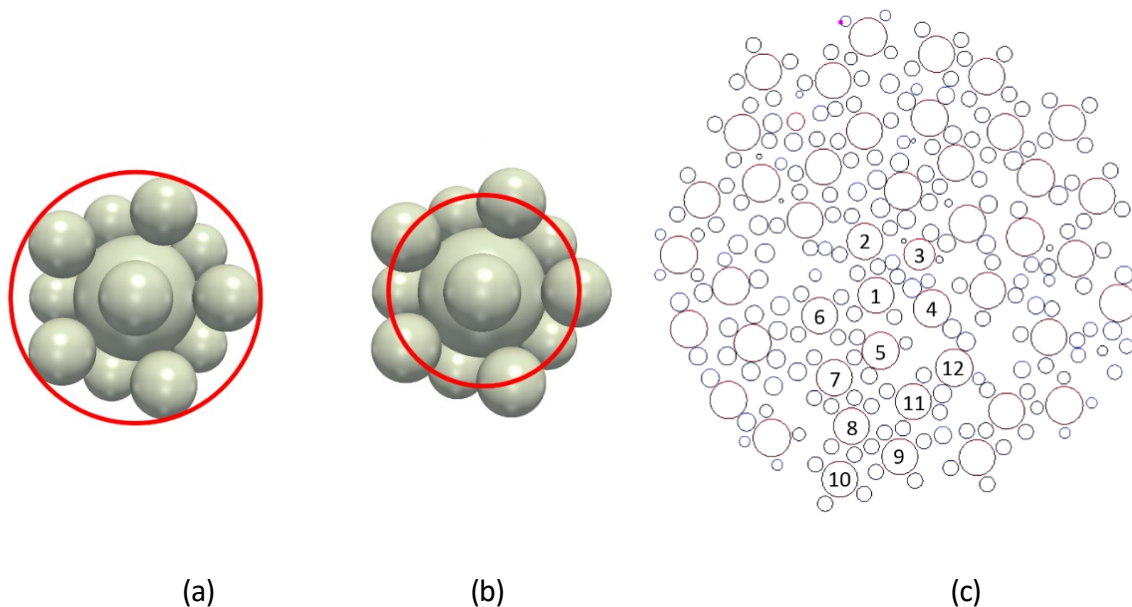


Figure 6 Methods to determine the size of multi-sphere particles: (a) envelope diameter, equivalent to 200 μm spherical particle; (b) diameter of the centres of the satellite particles; (c) measuring the distance between two multi-sphere particles in a DEM assembly.

Figure 6c illustrates the method of determining particle size from the distance between the central spheres. Several particle were selected and labelled as illustrated. The corresponding inter-particle distances are presented in Table 3. The minimum distance between two centres in the entire aggregate was determined. Accordingly the size of multi-sphere particle is equivalent to 137.23 μm . The average size calculated between neighbouring particles is equivalent to 168.615 μm . The

equivalent particle volume in this case gives the representative spherical particle size of 105.89 μm . In this work we use the method in Figure 6a.

Table 3 Distance between the centres of multi-sphere particles in a packing state shown in Figure 6c

Neighbour particle id	1-6	1-2	1-5	1-4	1-3	5-7	7-8	8-10	11-12
Centres distance, μm	149.5	145.9	152.8	142	168.8	139.3	145.5	143.1	137.2

1.3.3 Inter-particle friction

DEM permits the evaluation of a wide range of parameters influencing particle packing arrangements. The influence of both static and rolling friction on the packing density was studied for the 24 different shapes presented in Table 2. The overall structure of these multi-sphere particles were the same, one large particle in the middle (200 μm diameter) with a number of small particle of different diameters (25, 50, 75, 150, and 200 μm) distributed evenly on its surface. The only difference between these multi-sphere particles is the size and the number of the surrounding small particles. DEM studies were carried out by changing the friction coefficient while all other input parameters and insertion conditions were kept constant. The total number of the particles used in each test was based on a constant weight of powder of 4g. Table 4 shows the complete list of simulation inputs.

Table 4 Simulation input parameters for studies on the effect of friction

Constant Insertion mass	4 g
Number of particles	size dependent
Particle density (kg/m^3)	1500
Young's modulus (GPa)	1
Poisson's ratio	0.35
Coefficient of restitution	0.3
Static Friction Coefficient	0.0 – 1.0
Rolling Friction Coefficient	0.0 – 1.0
Surface energy	0

To determine the packing density a constant powder weight was used and the solid fraction was calculated based on the height of powder obtained from the simulation as shown in Figure 4b.

1.3.4 Surface energy

A parametric study based on varying the values of surface energy alongside with the coefficient of friction is conducted using values that cover the surface energy values reported in the literature for realistic powders. Three different shapes of multi-sphere particles as illustrated in Figure 7 were chosen to conduct this study. These shapes were selected based on the outputs of lowest packing density obtained from the test of friction coefficient introduced in Section 1.2.3. Each shape was tested for six different sizes (400, 300, 200, 100, 50, 25 μm) where the size in this case refers to the external particle diameter.

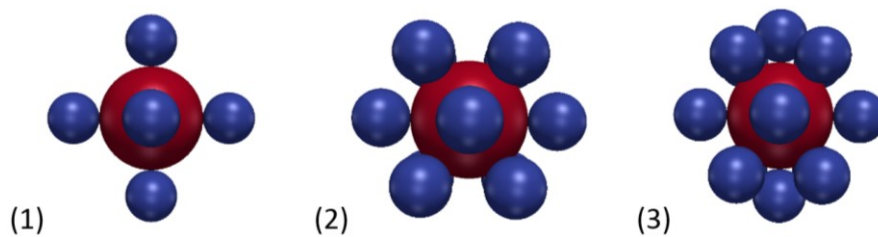


Figure 7 Three different shapes for multi-sphere particles used for packing density test for different surface energy values

To reduce the computational requirements and the simulation time and to keep the number of particles constant for all tests the size of the simulation domain was reduced consistently with the particle size. All other material proprieties were kept constant as in the previous test. Table 5 shows the list of simulation input parameters.

Table 5 Simulation input parameters for studies on the effect of surface energy

Number of multi-sphere particles	20,000
Particle size (μm)	400, 300, 200, 100, 50, 25
Particles density (kg/m^3)	1500
Young's modulus (GPa)	1
Poisson's ratio	0.35
Coefficient of restitution	0.3
Static Friction Coefficient	0.2, 0.3, 0.5 and 0.7
Rolling Friction Coefficient	0.1
Surface energy (mJ/m^2)	0, 10, 25 and 50

The surface energy values presented in Table 5 are representative the experimental measurements for real powders considered here [84, 85]. The solid volume fraction was calculated by selecting a domain of a given height as illustrated in Figure 4c and counting the number of particles within.

1.4 Results and discussion

DEM studies of the effects of particle shape, rolling and sliding friction and surface energy are presented below. The studies are designed to determine the conditions that lead to low packing density, representative to loosely packed quasi-spherical systems.

1.4.1 Preliminary studies

The solid fraction (SF) of spherical particles together with the three irregular shaped particles in Figure 5 are presented in Figure 8. In order to obtain low SF, these studies were conducted using a high (value 1) friction coefficient (detailed studies in the following section will show that high friction leads to lower SF). Thus the packing of the spherical particles is reduced to about 52%, however, the lowest packing is 45.5%, which is still significantly higher than the packing assemblies for real powders in Table 1 (0.2-0.3).

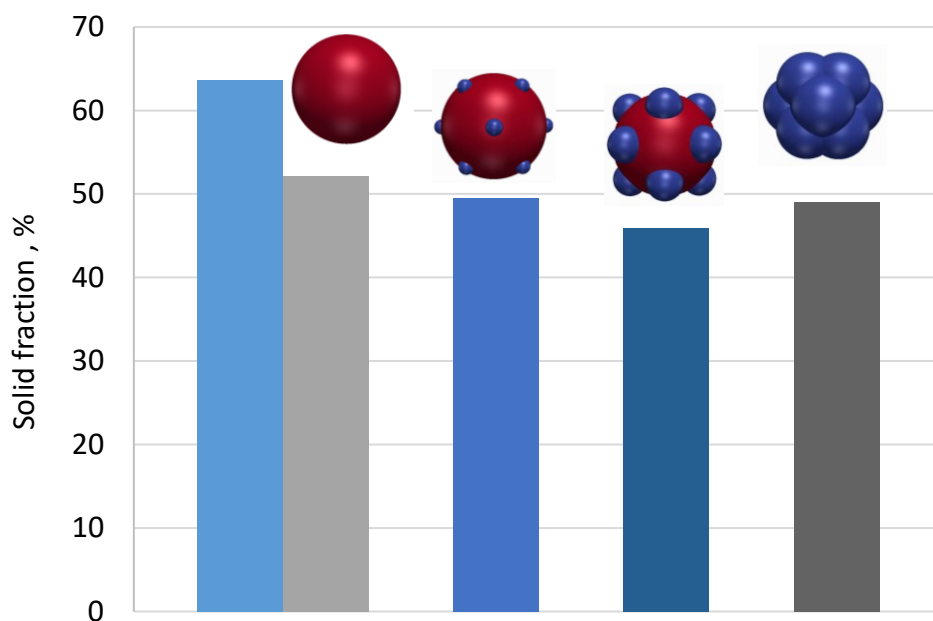
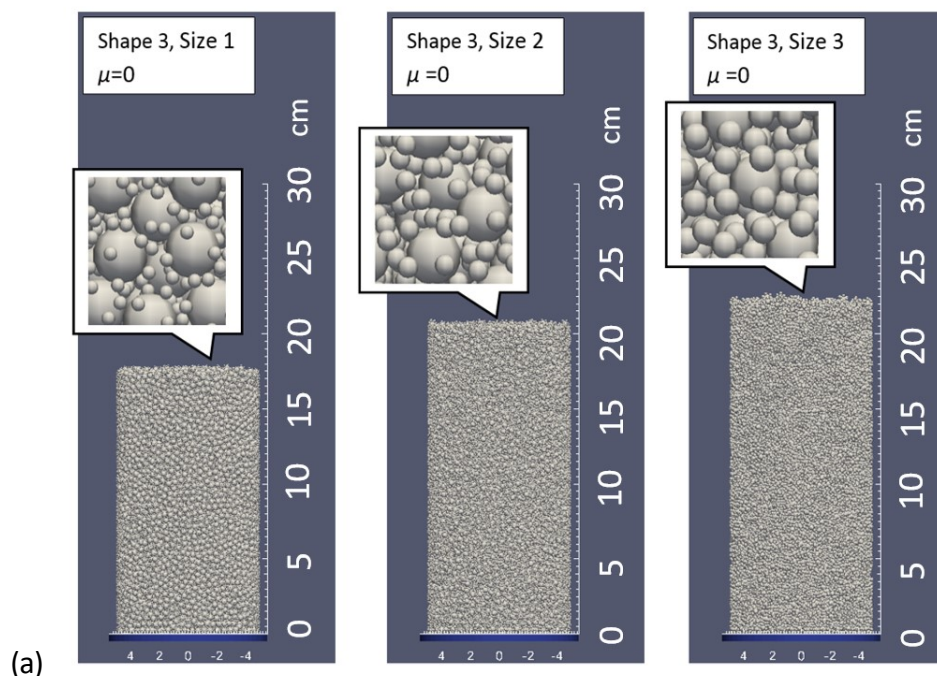


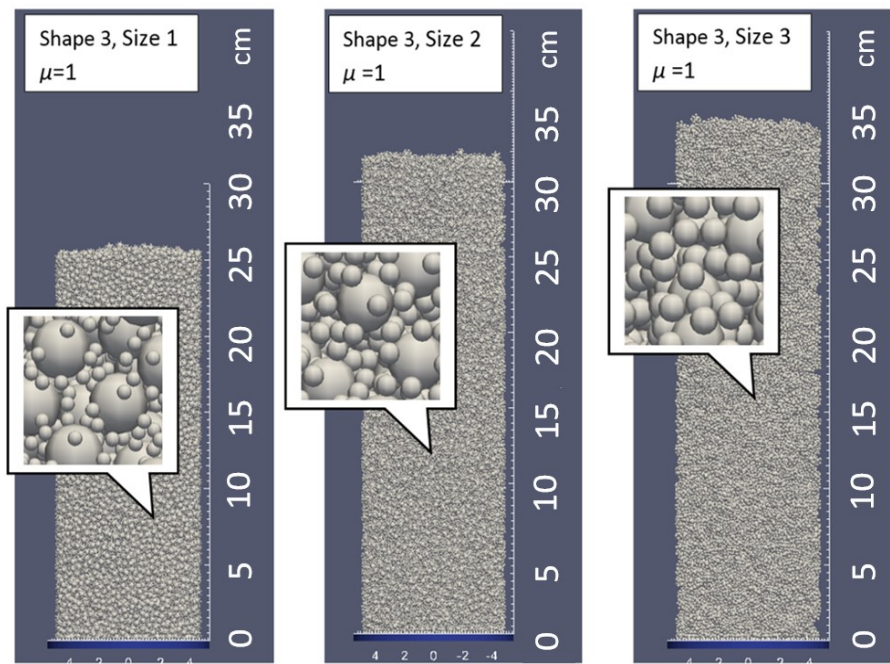
Figure 8 Solid fraction obtained for different overlapped multi-sphere particles. The 64% SF packing of spherical particles is shown for reference.

It is concluded that by designing overlapping particles the solid fraction can be manipulated, however, the SF still cannot be reduced to the measured values for loosely packed powders. The following qualitative explanation is given: the role of the satellites is to keep the centres apart. The minimum and maximum possible separation is thus the size of one or two satellites, respectively. Small satellites allow configurations that are closer to the lowest possible value while larger satellites, by filling the space completely provide shape closer to spherical, which gives high SF. These observations led to the design of particles in Table 2 and are explored systematically below.

1.4.2 Friction coefficients (static and rolling frictions combined) of 0 and 1 for all shapes

Simulations were conducted by firstly assigning the value of 0 for both static and rolling friction in all 24 cases shown in Table 2, then repeating the same simulation with a friction coefficient of the value of 1. The outputs of this study provide an indication of the range between the largest and smallest solid fraction that can be achieved using the considered shapes. This also helped to eliminate a number of cases which produced large SF, from the remaining of studies. Figure 9 presents a visualization of the simulation outputs for three different shapes at friction coefficients 0 and 1.

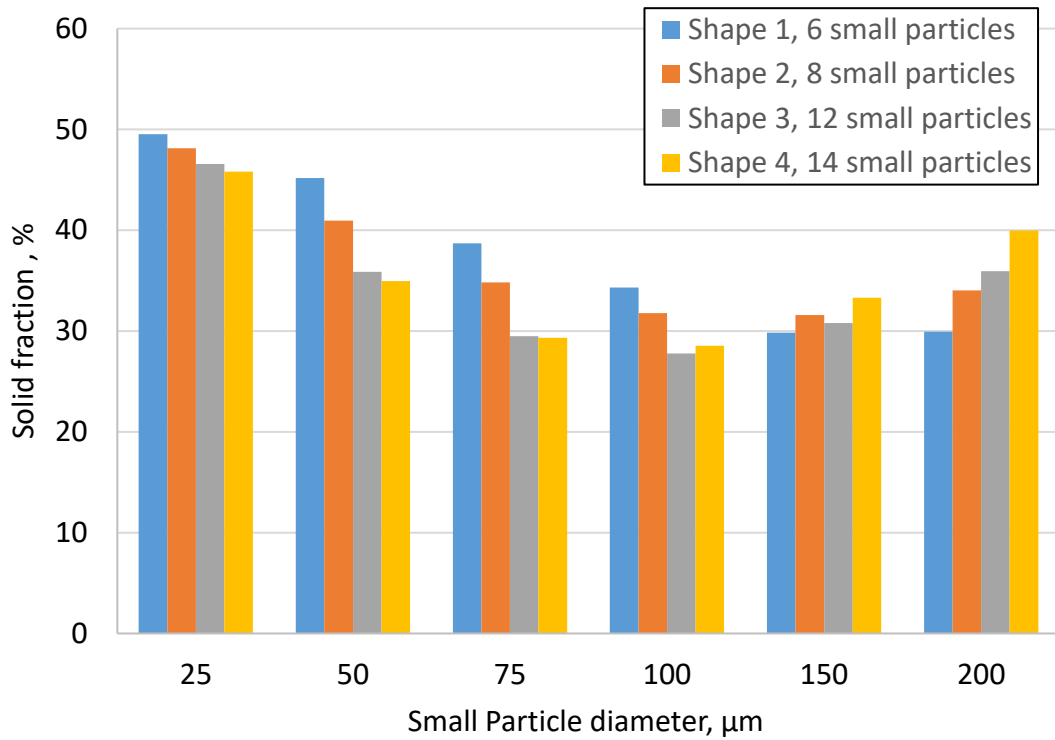




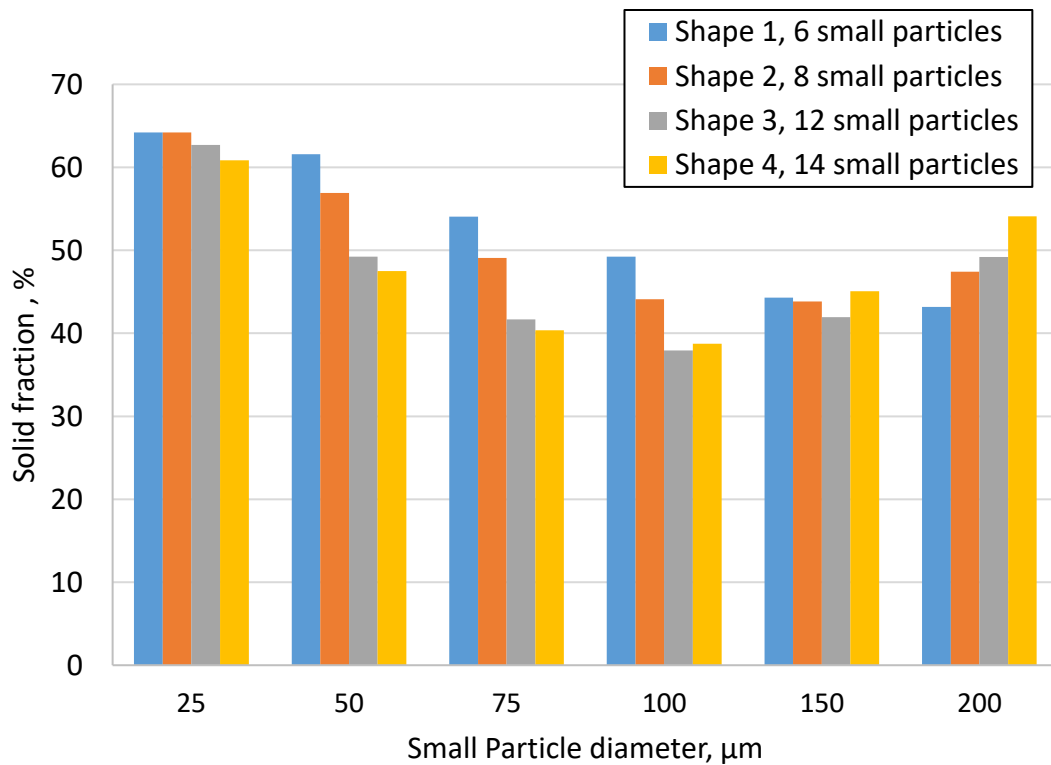
(b)

Figure 9 Simulation outputs for packing of three different shapes with the same total powder weight (Shape 3 sizes 1, 2, &3 in Table 2), a) frictionless case and b) friction coefficient 1

The simulation outputs in Figure 10, show a broad range of solid fractions obtained for the different cases. The overall trend displayed a reduction in solid fraction with the increase of satellite particle sizes from 25 to 100 μm , then this trend reversed as the sizes of surrounding particle increased from 100 to 200 μm . A similar trend was also observed when increasing the number of these small surrounding particles. The variety in SF almost typically exceeded 20%. For shape 1 with the small size satellite particles (25 μm), for instance, the solid fraction dropped from $\approx 50\%$ down to $\approx 30\%$ by increasing the size of these small particles to 150-200 μm . Similar tendency was detected for multi-sphere shape 3 where the solid fraction declined from about 47 % down to around 27 % by increasing the small particle sizes from 25 to 100 μm . It is also observed that using external particles as small as 25-50 μm did not affect the SF as much as the larger satellite particle sizes did. As an overall observation, three out of four of the studied shapes (1, 3, and 4) recorded a reduction in solid fraction down to about 30 % depending on the size of the satellite particles.



(a)



(b)

Figure 10 Solid fraction obtained for different multi-sphere particles with one sphere (200 μm) in the middle and small satellite particles with different sizes a) static and rolling friction of 1; b) static and rolling friction of 0

1.4.3 Static and rolling friction coefficients with special focus on the shape 3 (with 3 sizes)

Particle shape 3 (1 centred and 12 surrounding particles, Table 2) also referred to as “dodecahedron” shape, was one of the shapes that gave the most significant reduction in packing density in the previous analysis. Therefore, for pragmatic purposes, the following investigations were focused on this shape (taken three cases for small satellite particles).

In this test the friction coefficient and rolling friction values were decreased gradually from 1 to 0. As it can be seen in Figure 11 this reduction in friction values follows a similar drop in solid fraction with slightly higher decrease between 0 and 0.6 (e.g. from about 49.25 % to 37.91 % in case of multi-sphere particle diameter 0.3 mm) and small reductions afterwards between 0.6 and 1 (e.g. from 37.91 % to 35.88 % for the same particle diameter).

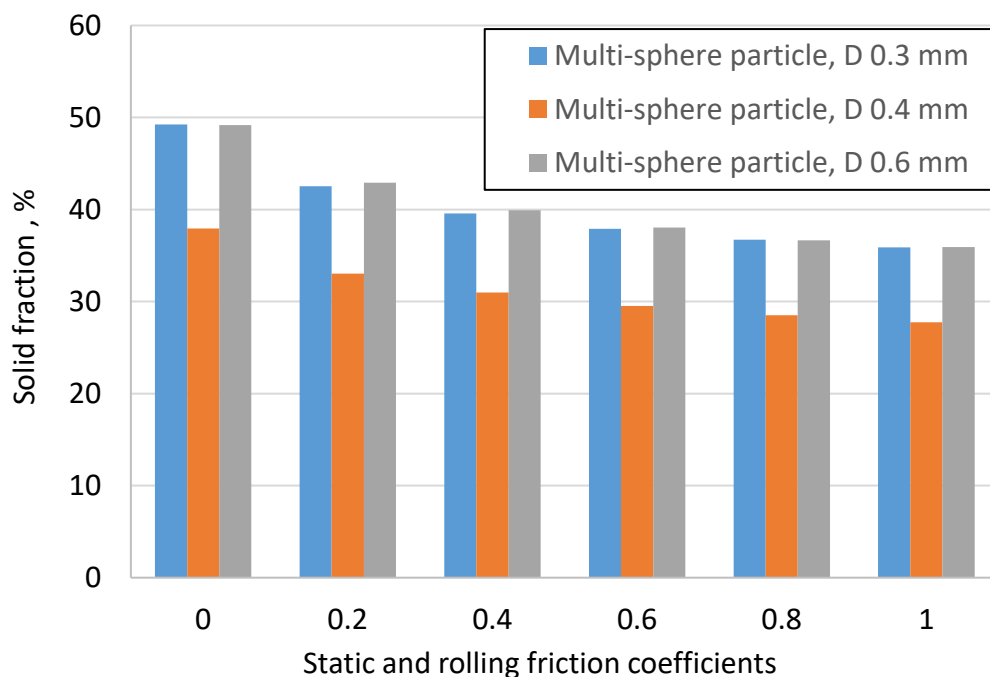


Figure 11 Solid fraction vs. friction coefficient (shape 3 in Table 2)

Figure 11 shows that the influence of friction value on solid fraction is more apparent for smaller friction coefficient values and this effect becomes less and less as the friction value exceeds 0.5. The other two multi-sphere particle sizes (0.4 and 0.6 mm diameter) demonstrated a similar SF reduction versus the values of the coefficient of friction.

1.4.4 Effect of static friction for shape 3 (with 3 sizes)

In order to determine whether the static friction or rolling friction coefficient has the highest influence on solid fraction, two separate tests were conducted. The value of the static friction coefficient was changed between 0-1 while the rolling friction was set to zero. Figure 12 shows that the solid fractions were similar to the solid fraction reduction obtained from the previous test with slightly higher SF value (overall less than 10%). For multi-sphere particle diameter 0.4 mm, for instance, the solid fraction reduction documented in the previous investigation was from 37.94% down to 27.76% (the lowest solid fraction obtained out of all studied cases), whereas in the current study the reduction was between 37.94 % to 29.76%. This shows that more than 90% of solid fraction decrease is due to the effect of static friction. It can be noted that this conclusion is drawn from studies where the particle systems was allowed to settle under the effect of gravity. For other processes the role of inter-particle friction may be different.

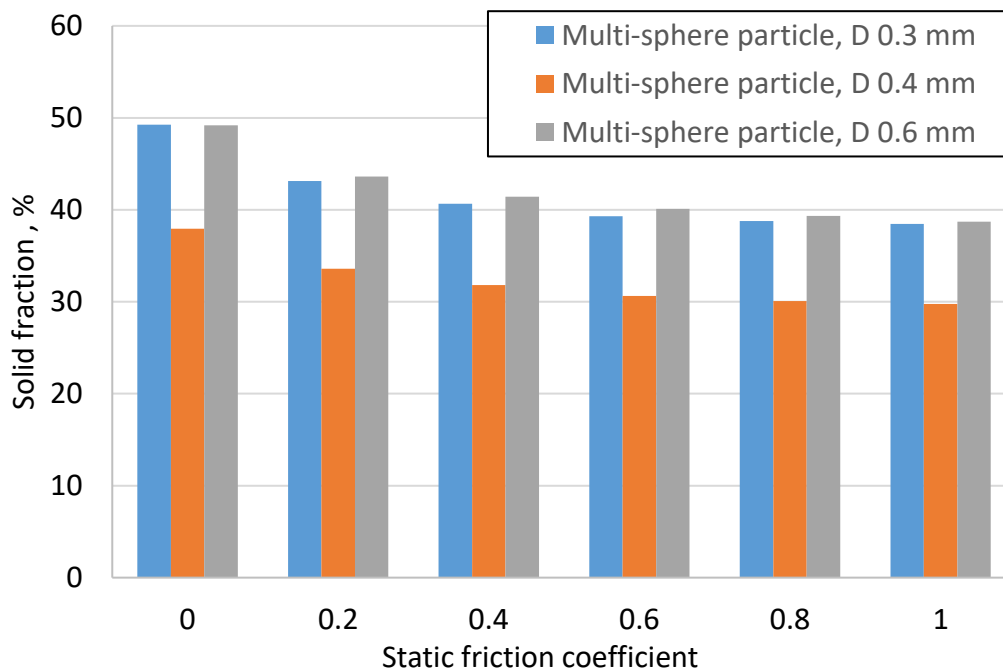


Figure 12 Solid fraction vs. friction coefficients at zero rolling friction

1.4.5 Effect of rolling friction for shape 3 (with 3 sizes)

In this study the static friction is fixed at zero and the rolling friction is varied between 0 - 1. Figure 13 illustrates the simulation outputs for SF changes based on rolling fraction variation. The solid fraction attained in this case displayed a different trend compare to the two previous tests with very small overall decrease in SF despite of rolling friction increase from 0 to 1. These findings are consistent with the observation made in the previous test in which the static friction was demonstrated to have the dominant influence.

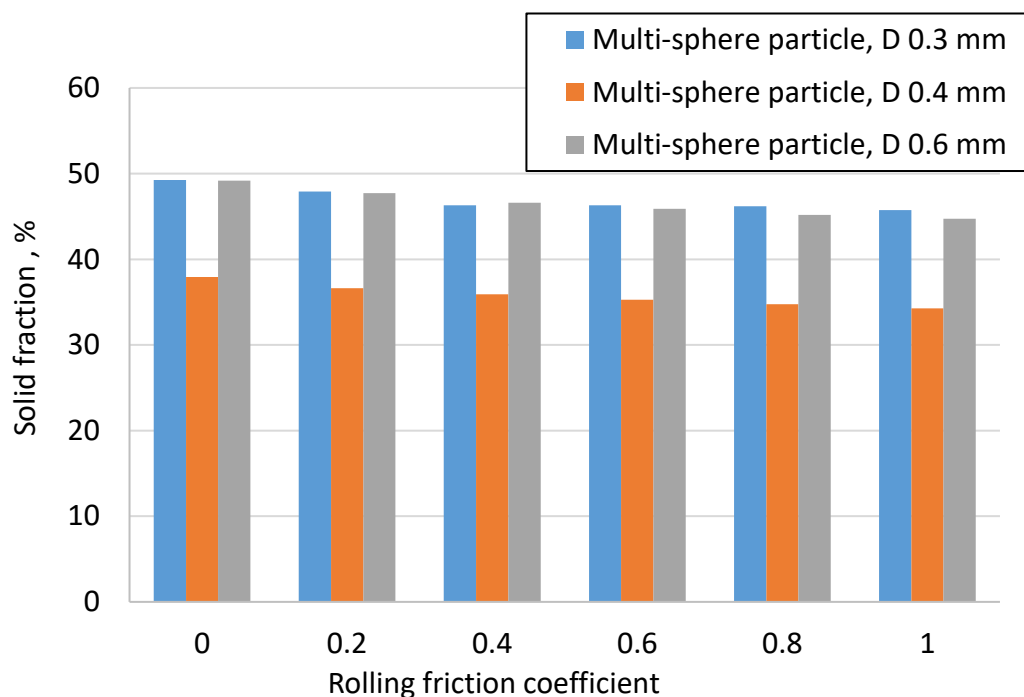


Figure 13 Solid fraction vs. rolling friction at zero friction coefficient

1.4.6 Surface energy

In this section surface energy is introduced in the analysis. As the particle size plays a more significant role in the presence of surface energy, these studies employ a wider range of particle sizes.

Figures 14, 15 and 16 present the solid fraction outputs for three different multi-sphere particles. Each shape was examined for six different sizes (400, 300, 200, 100, 50, 25 μm) with four different values for friction coefficients (0.2, 0.3, 0.5, 0.7) and surface energy (0, 10, 25, 50 mJ/m^2).

The outputs showed that in the absence of the adhesion, the solid fraction was approximately constant for all different particle sizes with the same shape. By applying cohesion to the system, the solid fraction decreases dramatically comparing to the no-cohesion case for the three applied cohesion values.

Friction plays a smaller role, and as in previous studies, SF decreases as the friction coefficient is increased. For example, the packing density obtained for the particle shape 1, size 400 μm , friction coefficient 0.2, and surface energy value of 25 mJ/m^2 was about 0.35 (Figure 14). By increasing the friction coefficient to 0.7 the solid fraction decreased to around 0.313.

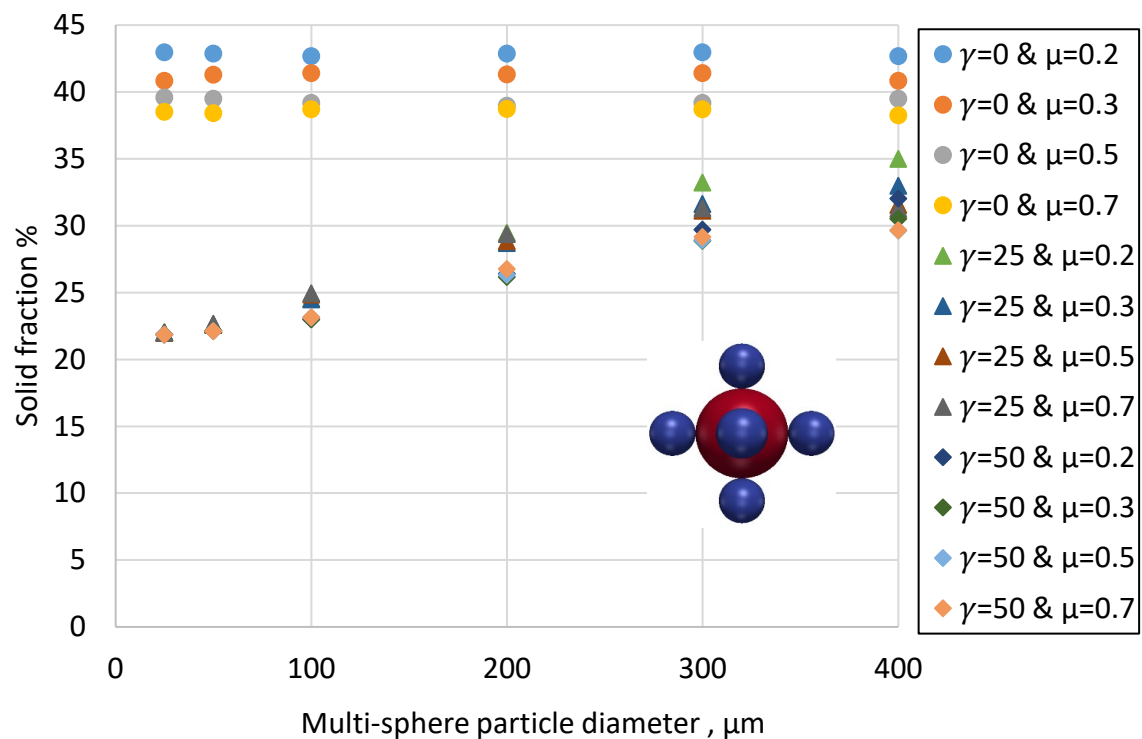
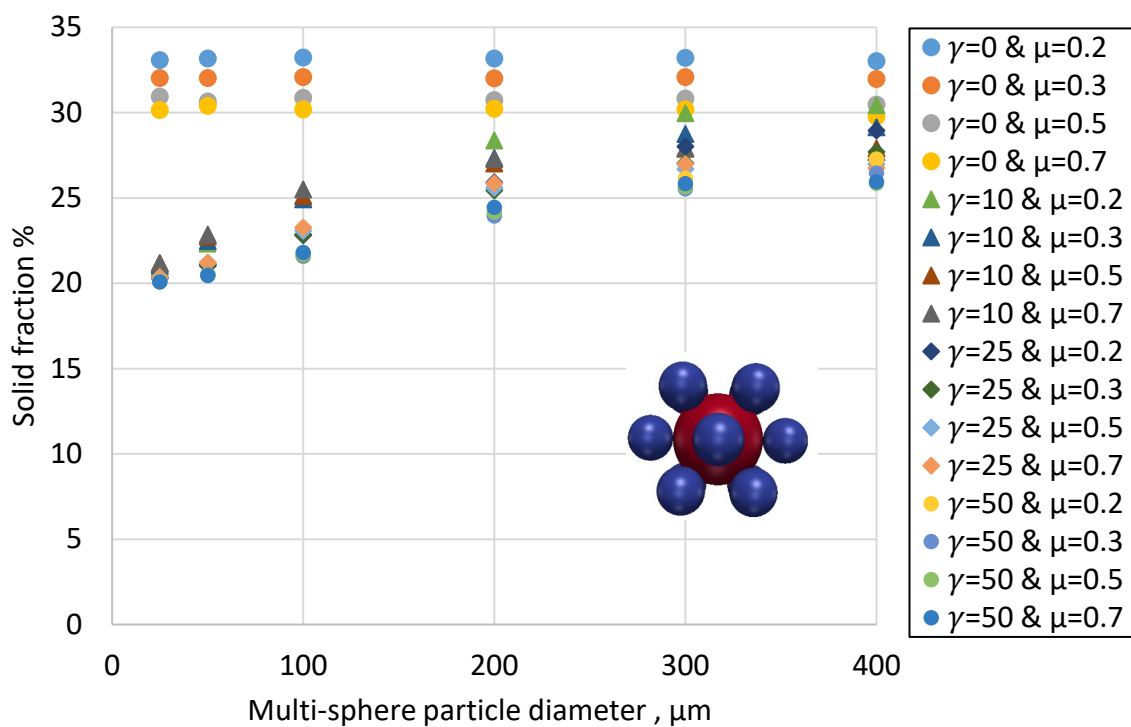
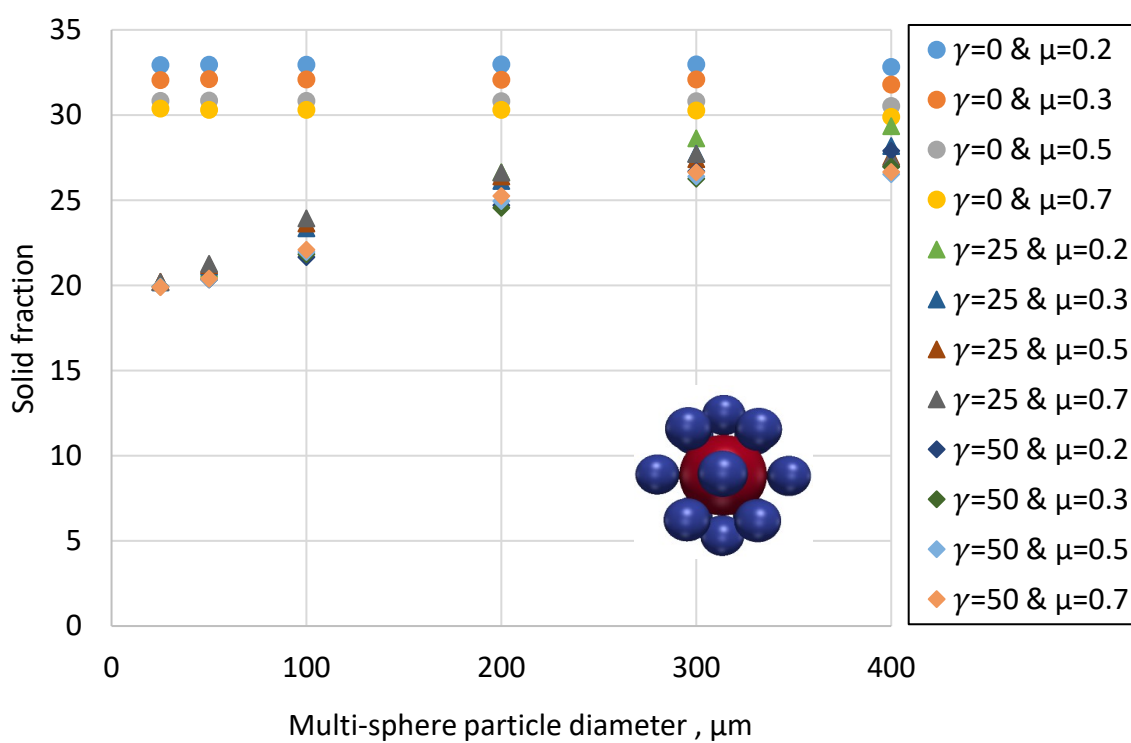


Figure 14 Solid fraction vs. surface energy and friction coefficient (Particle shape 1, size 4 in Table 2)



529

530 Figure 15 Solid fraction vs. surface energy and friction coefficient (Particle shape 3, size 4 in Table
531 2)



532

533 Figure 16 Solid fraction vs. surface energy and friction coefficient (Particle shape 4, size 4 in Table
534 2)

In case of smaller particles (e.g. 25 and 50 μm), however, changing the friction coefficient has almost no effect on solid fraction. With the same change in friction coefficient, for instance, the solid fraction was recorded between 0.225 and 0.226 for particle size 50 μm .

As the particle size is decreased, the surface energy becomes dominant in determining SF. For larger particles the friction has a notable influence, but the effect of friction almost completely disappears for small particles. Similar observations are drawn to the three particle shapes.

It is also important to highlight that the influence of surface energy on packing density is not unlimited. Looking at particle shape 3 (Figure 15) with size 200 μm and with friction coefficient 0.5, for instance, it can be seen that the bulk density decreases from 0.27 to 0.256 to finally 0.242 as the surface energy value increased from 10, up to 25, to 50 mJ/m^2 . This change in solid fraction is becoming smaller as the surface energy is increased.

1.5 Conclusions

This DEM study examined the factors affecting the packing of quasi-spherical particles. Specifically it explored the conditions under which low solid volume fractions of the order of ($\text{SF} = 0.3$), could be obtained. Such low packing density is typical for many powder materials, particularly fine and cohesive powders. The properties of commonly used pharmaceutical excipient powders were used for reference.

A range of quasi-spherical particle shapes consisting of a large central sphere surrounded by smaller spherical satellites were designed. These shapes resulted in lower packing density than the random packing of frictionless spherical assemblies ($\text{SF} = 0.64$), however, still considerably above the packing density of the practical powders used as reference. The packing density decreases as the diameter of the satellites is increased as more effective networks are formed to keep the central particles apart. The packing density also decreases as the number of satellites is increased, as such configurations prevent interlacing the satellites between neighbouring particles. Above a certain diameter and number of satellites, however, these trends reverse and as the particle shape becomes more spherical and the packing density increases towards that of spherical assemblies.

Increasing inter-particulate friction results in lower packing density. The studies on the effect of static and rolling friction show that static friction has a dominant influence on particle packing. More than 90% of solid fraction decrease is due to the effect of static friction. The packing density

is reduced as the friction coefficient was increased from 0-0.5, however above this value the SF reduction diminishes.

Adhesive interactions between particles were considered using the JKR adhesive contact law that requires surface energy as input. The role of adhesive forces increases as the particle diameter is decreased as is becoming dominant compared to the effect of friction and gravity. Friction continues to have an effect particularly for the larger particles, but as the particle size is decreased, the relative importance of friction vanishes and the packing is controlled by adhesive interactions and the geometry of the particles. Above a certain value of surface energy, however, the effect of adhesive interaction does not result in further reduction of packing density.

Finally, this work demonstrates that it is possible to obtain low packing densities ($SF = 0.3$), typical to small and cohesive powders, by considering, particle shape, size and inter-particle adhesion and friction. DEM studies reported in the literature are usually performed using spherical parties with properties calibrated to reproduce a given process (e.g. a dense particulate flow); however, in such analyses the solid fraction of the system is comparable to that of dense random packing of spheres, ($SF = 0.64$). The work presented in this paper demonstrated that by designing quasi-spherical particles, it is possible to obtain packing densities as low as $SF = 0.3$, typical to that of fine and cohesive powders. DEM studies employing such shapes benefit by being able to reproduce not only macroscopic behaviour (e.g. flow rate) but also capture the packing density of fine and cohesive particulate systems. As an example, the shapes designed in this work can be used to describe the flow and permeability behaviour of fine and cohesive powder [86].

1.6 Acknowledgement

H.E. would like to thank Aljabal Algharbi University in Libya/ Faculty of Engineering Jadu for presenting him with the opportunity to complete his PhD. He is also grateful to Libyan Cultural Affair in London for all the support and assistance given him during his PhD studies.

1.7 Conflict of interest

On behalf of all authors, the corresponding author states that there is no conflict of interest.

1.8 References

1. German, R.M., *Particle Packing Characteristics*. 1989: Metal Powder Industries Federation.

2. White, H.E. and S.F. Walton, *Particle Packing and Particle Shape*. Journal of the American Ceramic Society, 1937. **20**(1-12): p. 155 - 166.
3. *Chapter 4 Packing of Sedimentary Particles*, in *Developments in Sedimentology*, J.R.L. Allen, Editor. 1982, Elsevier. p. 137-177.
4. Rothon, R.N., *Particulate-Filled Polymer Composites*. 2003, Shawbury, Shrewsbury, Shropshire, SY4 4NR, UK: Rapra Technology Limited.
5. Dias, R., et al., *Particulate Binary Mixtures: Dependence of Packing Porosity on Particle Size Ratio*. Industrial & Engineering Chemistry Research, 2004. **43**(24): p. 7912-7919.
6. Sohn, H.Y. and C. Moreland, *The Effect of Particle Size Distribution on Packing Density*. The Canadian Journal of Chemical Engineering, 1968. **46**(3): p. 162-167.
7. Ye, X., et al., *Novel powder packing theory with bimodal particle size distribution-application in superalloy*. Advanced Powder Technology, 2018. **29**(9): p. 2280-2287.
8. Farr, R. and R. Groot, *Close packing density of polydisperse hard spheres*. The Journal of chemical physics, 2009. **131**: p. 244104.
9. Krupp, H., *Particle adhesion theory and experiment*. Advances in Colloid and Interface Science, 1967. **1**(2): p. 111-239.
10. Yu, A.B., J. Bridgwater, and A. Burbidge, *On the modelling of the packing of fine particles*. Powder Technology, 1997. **92**(3): p. 185-194.
11. Visser, J., *Van der Waals and other cohesive forces affecting powder fluidization*. Powder Technology, 1989. **58**(1): p. 1-10.
12. Bruni, G., *An investigation of the influence of fines size distribution and high temperature on the fluidization behaviour of gas fluidized beds linked with rheological studies*, in *Department of Chemical Engineering*. 2005, University College London London
13. Yu, A.B., N. Standish, and L. Lu, *Coal agglomeration and its effect on bulk density*. Powder Technology, 1995. **82**(2): p. 177-189.
14. Holubec, I. and E. D'Appolonia, *Effect of particle shape on the engineering properties of granular soils*. 1973: American Society for Testing and Materials.
15. Youd, T.L., *Factors controlling maximum and minimum densities of sands*. Evaluation of relative density and its role in geotechnical projects involving cohesion less soils, 1973(523).
16. Rouse, P., R.J. Fannin, and D.A. Shuttle, *Influence of roundness on the void ratio and strength of uniform sand*. Vol. 58. 2008. 227-231.
17. Cho, G.-C., J. Dodds, and J. Santamarina, *Particle Shape Effects on Packing Density, Stiffness, and Strength: Natural and Crushed Sands*. Geotechnical and Geoenvironmental Engineering, 2006. **132**(5): p. 591-602.
18. Nolan, G.T. and P.E. Kavanagh, *Random packing of nonspherical particles*. Powder Technology, 1995. **84**(3): p. 199-205.
19. Yang, R.Y., R.P. Zou, and A.B. Yu, *Effect of material properties on the packing of fine particles*. Journal of Applied Physics, 2003. **94**: p. 3025-3034.
20. Kallus, Y., *The random packing density of nearly spherical particles*. Soft Matter, 2016. **12**(18): p. 4123-4128.
21. Baserinia, R. and I.C. Sinka, *Mass flow rate of fine and cohesive powders under differential air pressure*. Powder Technology, 2018. **334**: p. 173-182.
22. Marigo, M. and E.H. Stitt, *Discrete Element Method (DEM) for Industrial Applications: Comments on Calibration and Validation for the Modelling of Cylindrical Pellets*. KONA Powder and Particle Journal, 2015. **32**: p. 236-252.

- 639 23. Ketterhagen, W.R., M.T. Ende, and B.C. Hancock, *Process Modeling in the Pharmaceutical*
640 *Industry using the Discrete Element Method*. Journal of Pharmaceutical Sciences, 2009.
641 **98**(2): p. 442-470.
- 642 24. Gantt, J.A. and E.P. Gatzke, *High-shear granulation modeling using a discrete element*
643 *simulation approach*. Powder Technology, 2005. **156**(2): p. 195-212.
- 644 25. Hassanpour, A., et al., *Effect of granulation scale-up on the strength of granules*. Powder
645 Technology, 2009. **189**(2): p. 304-312.
- 646 26. Wu, C.-Y., *DEM simulations of die filling during pharmaceutical tableting*. Particuology,
647 2008. **6**(6): p. 412-418.
- 648 27. Guo, Y., et al., *Numerical analysis of density-induced segregation during die filling*. Powder
649 Technology, 2010. **197**(1): p. 111-119.
- 650 28. Cleary, P.W. and M.L. Sawley, *DEM modelling of industrial granular flows: 3D case studies*
651 *and the effect of particle shape on hopper discharge*. Applied Mathematical Modelling,
652 2002. **26**(2): p. 89-111.
- 653 29. Anand, A., et al., *Predicting discharge dynamics from a rectangular hopper using the*
654 *discrete element method (DEM)*. Chemical Engineering Science, 2008. **63**(24): p. 5821-
655 5830.
- 656 30. Ketterhagen, W.R., et al., *Predicting the flow mode from hoppers using the discrete element*
657 *method*. Powder Technology, 2009. **195**(1): p. 1-10.
- 658 31. Arratia, P.E., et al., *A study of the mixing and segregation mechanisms in the Bohle Tote*
659 *blender via DEM simulations*. Powder Technology, 2006. **164**(1): p. 50-57.
- 660 32. Xu, Y., et al., *2D DEM simulation of particle mixing in rotating drum: A parametric study*.
661 Particuology, 2010. **8**(2): p. 141-149.
- 662 33. Alizadeh, E., F. Bertrand, and J. Chaouki, *Discrete element simulation of particle mixing and*
663 *segregation in a tetrapodal blender*. Computers & Chemical Engineering, 2014. **64**: p. 1-12.
- 664 34. Zhang, Z.P., et al., *A simulation study of the effects of dynamic variables on the packing of*
665 *spheres*. Powder Technology, 2001. **116**(1): p. 23-32.
- 666 35. Gan, J.Q., A.B. Yu, and Z.Y. Zhou, *DEM simulation on the packing of fine ellipsoids*. Chemical
667 Engineering Science, 2016. **156**: p. 64-76.
- 668 36. Cundall, P.A. and O. Strack, *A Discrete Numerical Mode For Granular Assemblies*. Vol. 29.
669 1979. 47-65.
- 670 37. Tanaka, K., et al., *Numerical and experimental studies for the impact of projectiles on*
671 *granular materials*, in *Handbook of Powder Technology*, A. Levy and H. Kalman, Editors.
672 2001, Elsevier Science B.V. p. 263-270.
- 673 38. Wills, B.A. and J.A. Finch, *Chapter 17 - Modeling and Characterization*, in *Wills' Mineral*
674 *Processing Technology (Eighth Edition)*, B.A. Wills and J.A. Finch, Editors. 2016,
675 Butterworth-Heinemann: Boston. p. 449-462.
- 676 39. Fortin, J., O. Millet, and G.d. Saxcé, *Numerical simulation of granular materials by an*
677 *improved discrete element method*. International Journal for Numerical Methods in
678 Engineering 2004. **62**: p. 639-663.
- 679 40. Mindlin, R.D., *Compliance of elastic bodies in contact*. Trans. ASME J. Appl. Mech., 1949.
680 **16**: p. 259-268.
- 681 41. Hertz, H., *Über die Berührung fester elastischer Körper*. Journal für die Reine und
682 Angewandte Mathematik, 1882. **92**: p. 156-171.
- 683 42. Johnson, K.L., K. Kendall, and A.D. Roberts, *Surface Energy and Contact of Elastic Solids*.
684 Vol. 324. 1971. 301-313.

- 685 43. Mishra, B.K., C. Thornton, and D. Bhimji, *A preliminary numerical investigation of*
686 *agglomeration in a rotary drum*. Minerals Engineering, 2002. **15**(1): p. 27-33.
- 687 44. Li, S.Q. and J.S. Marshall, *Discrete element simulation of micro-particle deposition on a*
688 *cylindrical fiber in an array*. Journal of Aerosol Science, 2007. **38**(10): p. 1031-1046.
- 689 45. Barthel, E., *Adhesive elastic contacts: JKR and more*. Journal of Physics D Applied Physics,
690 2008. **41**(16): p. 163001.
- 691 46. Deng, X., J.V. Scicolone, and R.N. Davé, *Discrete element method simulation of cohesive*
692 *particles mixing under magnetically assisted impaction*. Powder Technology, 2013. **243**: p.
693 96-109.
- 694 47. Deng, X.L. and R.N. Davé, *Dynamic simulation of particle packing influenced by size, aspect*
695 *ratio and surface energy*. Granular Matter, 2013. **15**(4): p. 401-415.
- 696 48. Cabiscol, R., J.H. Finke, and A. Kwade, *Calibration and interpretation of DEM parameters*
697 *for simulations of cylindrical tablets with multi-sphere approach*. Powder Technology,
698 2018. **327**: p. 232-245.
- 699 49. Asaf, Z., D. Rubinstein, and I. Shmulevich, *Determination of discrete element model*
700 *parameters required for soil tillage*. Soil and Tillage Research, 2007. **92**(1): p. 227-242.
- 701 50. Coetzee, C.J., *Review: Calibration of the discrete element method*. Powder Technology,
702 2017. **310**: p. 104-142.
- 703 51. Coetzee, C.J., *Particle upscaling: Calibration and validation of the discrete element method*.
704 Powder Technology, 2019. **344**: p. 487-503.
- 705 52. Fangping, Y., et al., *Calibration and verification of DEM parameters for dynamic particle*
706 *flow conditions using a backpropagation neural network*. Advanced Powder Technology,
707 2019. **30**(2): p. 292-301.
- 708 53. Roessler, T. and A. Katterfeld, *DEM parameter calibration of cohesive bulk materials using*
709 *a simple angle of repose test*. Particuology, 2019.
- 710 54. Boikov, A., R. Savelev, and V. Payor, *DEM Calibration Approach: Random Forest*. Journal of
711 Physics, 2018. **1118**: p. 012009.
- 712 55. Coetzee, C.J., *Calibration of the discrete element method and the effect of particle shape*.
713 Powder Technology, 2016. **297**: p. 50-70.
- 714 56. Do, H.Q., A.M. Aragón, and D.L. Schott, *A calibration framework for discrete element model*
715 *parameters using genetic algorithms*. Advanced Powder Technology, 2018. **29**(6): p. 1393-
716 1403.
- 717 57. Baroutaji, A., et al., *Mechanics and Computational Modeling of Pharmaceutical Tabletting*
718 *Process*, in *Reference Module in Materials Science and Materials Engineering*. 2017,
719 Elsevier.
- 720 58. Lemieux, M., et al., *Large-scale numerical investigation of solids mixing in a V-blender using*
721 *the discrete element method*. Powder Technology, 2008. **181**(2): p. 205-216.
- 722 59. Bertrand, F., L.A. Leclaire, and G. Levecque, *DEM-based models for the mixing of granular*
723 *materials*. Chemical Engineering Science, 2005. **60**(8): p. 2517-2531.
- 724 60. Roskilly, S.J., et al., *Investigating the effect of shape on particle segregation using a Monte*
725 *Carlo simulation*. Powder Technology, 2010. **203**(2): p. 211-222.
- 726 61. Miyajima, T., K.-I. Yamamoto, and M. Sugimoto, *Effect of particle shape on packing*
727 *properties during tapping*. Advanced Powder Technology, 2001. **12**(1): p. 117-134.
- 728 62. Zhao, S., et al., *Particle shape effects on fabric of granular random packing*. Powder
729 Technology, 2017. **310**: p. 175-186.
- 730 63. Anikeenko, A.V. and N.N. Medvedev, *Polytetrahedral Nature of the Dense Disordered*
731 *Packings of Hard Spheres*. Physical Review Letters, 2007. **98**(23): p. 235504.

64. Klumov, B.A., S.A. Khrapak, and G.E. Morfill, *Structural properties of dense hard sphere packings*. Physical Review B, 2011. **83**(18): p. 184105.
65. Onoda, G.Y. and E.G. Liniger, *Random loose packings of uniform spheres and the dilatancy onset*. Physical Review Letters, 1990. **64**(22): p. 2727-2730.
66. Jerkins, M., et al., *Onset of Mechanical Stability in Random Packings of Frictional Spheres*. Physical Review Letters, 2008. **101**(1): p. 018301.
67. Farrell, G.R., K.M. Martini, and N. Menon, *Loose packings of frictional spheres*. Soft Matter, 2010. **6**: p. 2925-2930.
68. Kloss, C., et al., *Models, algorithms and validation for opensource DEM and CFD-DEM*. Progress in Computational Fluid Dynamics, An International Journal, 2012. **12**(2/3): p. 140.
69. GARCIA, X., et al., *A clustered overlapping sphere algorithm to represent real particles in discrete element modelling*. Géotechnique, 2009. **59**(9): p. 779-784.
70. Lu, G., J.R. Third, and C.R. Müller, *Discrete element models for non-spherical particle systems: From theoretical developments to applications*. Chemical Engineering Science, 2015. **127**: p. 425-465.
71. You, Y. and Y. Zhao, *Discrete element modelling of ellipsoidal particles using super-ellipsoids and multi-spheres: A comparative study*. Powder Technology, 2018. **331**: p. 179-191.
72. He, Y., et al., *Discrete modelling of the compaction of non-spherical particles using a multi-sphere approach*. Minerals Engineering, 2018. **117**: p. 108-116.
73. Seelen, L.J.H., J.T. Padding, and J.A.M. Kuipers, *A granular Discrete Element Method for arbitrary convex particle shapes: Method and packing generation*. Chemical Engineering Science, 2018. **189**: p. 84-101.
74. Tahmasebi, P., *Packing of discrete and irregular particles*. Computers and Geotechnics, 2018. **100**: p. 52-61.
75. Majidi, B., et al., *Packing density of irregular shape particles: DEM simulations applied to anode-grade coke aggregates*. Advanced Powder Technology, 2015. **26**(4): p. 1256-1262.
76. Gan, J.Q., Z.Y. Zhou, and A.B. Yu, *Interparticle force analysis on the packing of fine ellipsoids*. Powder Technology, 2017. **320**: p. 610-624.
77. Tangri, H., Y. Guo, and J.S. Curtis, *Packing of cylindrical particles: DEM simulations and experimental measurements*. Powder Technology, 2017. **317**: p. 72-82.
78. Parteli, E.J.R., et al., *Attractive particle interaction forces and packing density of fine glass powders*. Scientific reports, 2014. **4**: p. 6227-6227.
79. Liu, W., et al., *Adhesive loose packings of small dry particles*. Soft Matter, 2015. **11**(32): p. 6492-6498.
80. Liu, W., et al., *Effects of hydrodynamic interaction on random adhesive loose packings of micron-sized particles*. EPJ Web Conf., 2017. **140**: p. 08017.
81. Thornton, C., S.J. Cummins, and P.W. Cleary, *An investigation of the comparative behaviour of alternative contact force models during inelastic collisions*. Powder Technology, 2013. **233**: p. 30-46.
82. Elmsahli H. S. M., *Numerical Analysis of Powder Flow using Computational Fluid Dynamics Coupled with Discrete Element Modelling*. 2019. PhD thesis, university of Leicester.
83. Rhodes, M., *Introduction to particle technology* 2008, John Wiley & Sons: Great Britain.
84. Ho R., Hinder S.J., Watts J.F., Dilworth S.E., Williams D.R., Heng JYY, 2010. Determination of surface heterogeneity of d-mannitol by sessile drop contact angle and finite concentration inverse gas chromatography. International Journal of Pharmaceutics, Volume 387, Issues 1–2, Pages 79-86, <https://doi.org/10.1016/j.ijpharm.2009.12.011>.

- 778 85. Karde V., Ghoroi C., 2014. Influence of surface modification on wettability and surface
779 energy characteristics of pharmaceutical excipient powders. International Journal of
780 Pharmaceutics. Volume 475, Issues 1–2, Pages 351-363,
781 <https://doi.org/10.1016/j.ijpharm.2014.09.002>.
- 782 86. Elmsahli H.S. and Sinka I.C. Coupled CFD-DEM analysis of mass flow rate of fine and
783 cohesive powders under differential air pressure. International Journal of Solids and
784 Structures. Manuscript submitted 2 November 2019, under review.